The Distribution of Gas Densities in the Milky Way

Stefan O'Dougherty   College of Liberal Arts and Sciences, University of Florida

Observations of the atomic and molecular phases of the interstellar medium that coincide with the 20° by 6° region covered by the Census of High- and Medium-mass Protostars survey (CHaMP; Barnes et al. 2011) are used to derive mass estimates and a probability distribution function of gas with density. The Southern Galactic Plane Survey (SGPS; McClure-Griffiths et al. 2005) and The Galactic All Sky Survey (GASS; McClure-Griffiths et al. 2009) were used for the HI, while the Nanten surveys (Yonekura et al. 2005) of ^{12}CO, ^{13}CO, C^{18}O and HCO$^+$ were used as tracers for H$_2$. Maximum and minimum mass estimates for each of the surveys were calculated due to the distance ambiguity that occurs within the solar radius. The derived probability distribution function is compared to simulations of a model galaxy (Tasker & Tan 2009; Tasker 2011). Maps of the distribution of the mass were generated as viewed from above the Milky Way for the 20° Galactic longitude range covered by CHaMP in each of the surveys for a better understanding of the distribution of GMCs and the structure of any spiral arms in the region.

Introduction

From stars to the diffuse matter that lies between them, the universe is composed primarily of hydrogen. Within the confines of the local Milky Way, hydrogen exists in three states: atomic (HI), molecular (H$_2$), and ionized. The HI accounts for roughly 75% of gas mass, while the remainder is H$_2$ and a small fraction of gas that is ionized. The H$_2$ gas exists as structures known as Giant Molecular Clouds (GMCs), which are the sites of star formation. By studying these clouds, insight can be gained on the complex processes that are involved with star formation. For example, radio surveys of the HI 21 cm line and H$_2$ molecular tracers can be used to study the distribution of the mass among various density domains within these GMCs. This distribution is an important constraint when creating theoretical models of GMC formation in spiral galaxies like our own Milky Way.

A section of the Galaxy covering parts of Vela, Carina, and Centaurus was chosen for the purposes of this mass analysis since the area has been covered by some of the latest and highest resolution surveys dedicated to map GMCs on a large scale. The Census of High- and Medium-mass Protostars (CHaMP; Barnes et al. 2011) has a coverage of 20° by 6° over this southern region of the Milky Way. CHaMP surveys the region using several tracers of different densities in a more complete and unbiased way than previous surveys to further enhance knowledge of the physical processes involved with star formation.

This survey can be complemented by investigating the amount of mass for the atomic and molecular gas in the region. Analysis of the HI and H$_2$ molecular tracers that cover different densities can lead to the computation of a probability distribution function of gas with density (gas density PDF) that gives the mass fractions for each molecular tracer as a function of density. Theoretical

models of the evolution of the Milky Way's interstellar medium (Tasker & Tan 2009; Tasker 2011) with their own gas density PDF can then be used as a comparison with the observational data to evaluate theories of formation and properties of the GMCs.

The CHaMP region is between Galactic longitudes 280° to 300°, Galactic latitudes -4° to 2° and covers the frequency ranges of 85 to 93 GHz and 107 to 115 GHz. CHaMP uses the Australia Telescope National Facility's 22 meter diameter Mopra antenna and the MOPS digital filterbank to acquire high resolution maps, with a beam size of 40", on numerous spectral lines in the region. The CHaMP survey has identified 209 clumps (Barnes et al. 2011) based on the Nanten surveys conducted in the same area. The Nanten survey (Yonekura et al. 2005; Fukui et al. 2008) was conducted using a recursive mapping technique that covered the H$_2$ molecular tracers of ^{12}CO, ^{13}CO, C^{18}O and HCO$^+$. Each tracer probes denser components of molecular gas, thus the ^{12}CO was used as a finder chart for mapping out the ^{13}CO, then the latter used as a basis for mapping out the C^{18}O. This technique allows for unbiased sampling of the entire region, since the majority of all active star formation is traceable from C^{18}O emission. For this research, the mass properties of the entire region from the Nanten survey will be combined with the results from the detailed core study. In contrast to CHaMP, Nanten has a lower angular resolution of 3.3' and a velocity resolution of 0.1 km s^{-1}, however the cubes used in this analysis had lower velocity resolutions of 0.5 and 1 km s^{-1}.

In order to calculate the mass of HI in the region two surveys were selected: the Southern Galactic Plane Survey (SGPS; McClure-Griffiths et al. 2005) and the Galactic All Sky Survey (GASS; McClure-Griffiths et al. 2009). The SGPS has a higher angular resolution of 2.2'; however, it only covers |b| ≤ 1.5°. To complete the full coverage of the CHaMP region the missing data is taken from the GASS survey at an angular resolution of 16' for the latitudes not

covered by the SGPS. The velocity resolution of both is equivalent at 0.82 km s^{-1}.

Techniques

Data from the SGPS, GASS, and Nanten surveys were used to calculated masses for the HI and the tracers of H_2. An initial assumption of a flat rotation curve is made in determining the distances of the signal that adopts the values $R_0 = 8.4$ kpc and $\Theta_o = 254$ km s^{-1} (Reid et al. 2009). One major problem that affects the calculation of the mass is the distance ambiguity, brought about by our location within the disk of the Milky Way. For any V_{LSR} that corresponds to $R < R_0$, a distance ambiguity arises. It is impossible to determine whether the mass being calculated is located at the near or the far distance based on the V_{LSR} alone. In an attempt to remedy this, for one calculation it is assumed the distance is near every time $R < R_0$, and for the second calculation the far distance is applied. As Table 1 shows, an upper and lower limit then exists for each tracer, the average of which is used for the gas density PDF.

The initial mass calculation starts with the determination of the column density for each survey. In general form the column density along each line of sight is calculated via

$$N_a = Y_a \int T \, dv \qquad (1)$$

$$\text{and} \qquad N_{H2} = X_a \, N_a \qquad (2)$$

where a is specific to the particular tracer, Y_a is the scaling factor from the observed intensity to column density of that tracer, while X_a scales directly to the H column density (whether atomic or molecular), and T is the brightness temperature measured. Assuming optically thin conditions, we use $Y_H = 1.8 \times 10^{18}$ cm^{-2} K^{-1} km^{-1} s for the HI (Spitzer 1978) which is calculated independent of temperature. For the ^{12}CO we adopt $X_{12CO} = 1.8 \times 10^{20}$ cm^{-2} K^{-1} km^{-1} s (Dame et al. 2001). In order to convert the ^{13}CO we use $N_{H2} = 1.0 \times 10^4 \, N_{12CO}$ and $N_{12CO} = 70 \, N_{13CO}$ with $Y_{13CO} = 8.76 \times 10^{14}$ cm^{-2} K^{-1} km^{-1} s. The $C^{18}O$ uses $N_{12CO} = 560 \, N_{C18O}$ with $Y_{C18O} = 1.16 \times 10^{15}$ cm^{-2} K^{-1} km^{-1} s.

The HCO$^+$ (J=1$\rightarrow$0) column density is calculated via,

$$N(HCO^+) = \frac{3h}{8\pi^3\mu^2_D J_u} \frac{Q(T_{ex})\exp(E_u/kT_{ex})}{(1-\exp(h\nu/kT_{ex}))} \int \tau \, dV \quad (3)$$

where Q is the partition function calculated at a T_{ex} of 10 K, and J_u, E_u are calculated for the upper level, J=1. The optical depth τ is then calculated at each point using,

$$\tau = -\ln(1 - T_{mb} /(T_{ex} - T_{bg})) \qquad (4)$$

where T_{mb} is the main beam temperature from the data cube, T_{ex} is 10 K and T_{bg} is 2.73 K.

Along each line of sight the column densities are converted into a mass surface density and summed over the entire region for a final mass result with the general equation,

$$M_{total} = \sum (m_H\mu_p A N_a) \qquad (5)$$

where N_a is the column density, m_H is the mass of hydrogen, $\mu_p = 1.4$ or 2.8 is the mean mass per particle for atomic or molecular gas respectively and accounts for the helium abundance in the gas and A is equal to the pixel's projected area times the distance squared.

Besides having the Nanten HCO$^+$ data, the CHaMP HCO$^+$ data is available for the same region (Barnes et al. 2011, hereafter Paper I). As a comparison between the two data sets, several additional methods of calculating the mass for the CHaMP sources and the whole region were conducted. The mass of HCO$^+$ in Table 1 is from the Nanten survey and has been calculated as described above. The following comparisons are summarized in Table 2.

Paper I has defined 301 clumps, from 121 Nanten clumps, and their respective masses through a two dimensional Gaussian fit model. Their locations, masses, and other properties are all listed in Paper I. As an initial comparison to this Gaussian fit model, a script was written to calculate the mass of each of these clumps that summed up all the signal, as opposed to fitting a Gaussian, in a defined ellipse. Paper I has quoted half power ellipse sizes and in order to pick up the majority of the signal, an ellipse a factor of two times the quoted size was taken and all the mass within summed. In order to have the same basis for comparison the same velocity range, based on a 3σ velocity range from the peak V_{LSR} of the source, is applied as a constraint. The majority of clumps have associated sources with previously known distances that help to resolve the distance ambiguity, therefore the quoted distances from Paper I were applied instead of calculating a kinematic distance to each clump.

Another method of comparison of the Gaussian mass method included summing up all emission in the HCO$^+$ Paper I dataset, not simply limiting it to the defined source ellipses. Velocity and distance constraints unique to each region were applied. In an effort to minimize noise caused by edge pixels, noisier regions and noisier strips within regions, only signal with intensity 3σ above the mean noise as calculated over a line free region for each position was counted.

When comparing the HCO+ coverage of Nanten to Mopra, the former will actually be covering a larger area, but at a poorer resolution. In order to compare the difference in the surveys, the calculation of the mass of the Nanten data was split during calculation in longitude space to match corresponding CHaMP regions. The velocities from the CHaMP sources that overlapped within these longitude slices were separated and had their mass calculated using the same distances as the defined in Paper

I. This allowed for a total mass of just the overlapping regions to be calculated, in addition to limiting the amount of distance ambiguity in the Nanten HCO+ mass total.

As a supplement to calculating the mass of the HI and H_2, information on the distances and the corresponding longitudinal pixels were saved for each mass run, which allowed for overhead maps of the gas distributions to be plotted. They have been split into 0.5 x 0.5 kpc bins along each longitude point. The corresponding longitude and distance were then plotted onto a polar coordinate system with a contour overlay of the mass density in terms of $M_\odot$ pc^{-2} to illustrate the structure of the GMCs and the arms in which they are found.

Results

The initial mass results are shown in Table 1 in units of 10^6 $M_\odot$. Listed for the HI is the amount of mass in the SGPS survey, the amount in the higher latitudes of the GASS survey, and the total amount of HI across the full range. Each tracer has a calculation for the amount of mass within the solar radius using the near distance, the far distance, and an average of the two. Column 4 gives the total mass outside the solar radius, for which there is only one solution for the kinematic distance. Column 5 gives the total mass based on the average of the near & far distances and the total outside mass.

Comparing the average total of the SGPS and the GASS with $|b| \leq 1.5°$ yields a difference of ~5 x 10^6 $M_\odot$, which corresponds to a ~4% difference between the mass totals. This a reasonably small and acceptable difference between the two surveys considering the difference in resolution (2.2' vs 16').

For the gas density PDF, only mass that falls within a distance of 8 kpc is taken into account. As illustrated in the overhead maps in Figure 3, the majority of the mass across all tracers falls within 8 kpc. For the molecular tracers, there is no mass detected by the surveys above their sensitivity levels past 10 kpc. Furthermore, for the weaker emission of $C^{18}O$ and HCO^+, the noise tends to dominate over any actual emission in the outer regions, leading to slightly negative results past 8 kpc. Limiting the radius to 8 kpc thus helps limit the weaker emission and is justifiable as a reasonable cutoff point for comparisons between the HI and the H_2.

Table 1: Mass Totals for each survey in units of 10^6 $M_\odot$. Results are divided into interior and outer totals, to illustrate the effect of the distance ambiguity. Column 5 lists the total mass values using the interior average and the outer mass.

	Interior Near	Interior Far	Interior Average	Outer	Total
HI $_{Total}$	10.53	34.57	22.58	230.42	253.00
HI $_{SGPS}$	5.40	18.48	11.94	110.75	122.69
HI $_{GASS}$ $|b| < 1.5°$	5.05	17.61	11.36	106.43	117.79
^{12}**CO** $_{Nanten}$	2.95	6.16	4.56	7.85	12.41
^{13}**CO** $_{Nanten}$	1.27	2.62	1.94	2.52	4.46
C^{18}**O** $_{Nanten}$	0.56	1.13	0.84	0.46	1.30
HCO$^+$ $_{Nanten}$	0.122	0.129	0.126	0.145	0.271

Table 2: Comparison of Nanten and HCO+ mass calculated through various methods. Refer to Section II for more information on the specific differences between each method.

Source & Method	Mass (10^6 $M_\odot$)
CHaMP Sources 2D Gaussian Method	0.219
CHaMP Sources Summed Intensity Method	0.263
Entire Mopra Cubes Method	0.268
Entire Nanten Cubes Method	0.541
Nanten Limited to CHaMP Region Method	0.336

With the above limit imposed, the final gas density PDF is calculated and can be seen in Figure 1. The mass fractions are plotted over a range of densities thought to be associated with their respective tracer. The Mopra data does have a calculated weighted mean density, however the other ranges are our best estimates. We also include error bars for each tracer, taking into account the ambiguities

associated with the distance, a flat rotation curve, column density calculations, and conversion factor uncertainties.

The molecular tracers in general have all their mass located within 8 kpc, so a larger percentage of their mass falls within the solar radius than for the atomic mass. Therefore, for the H_2 tracers the distance ambiguity uncertainty ranges from 13% to 18%; however, the HI uncertainty is only 5%. To estimate the uncertainty for assuming a flat rotation curve, the velocity used to calculate a distance at a specific longitude was varied by +/-10 km s^{-1} to see the resulting change in mass. They all vary between 2-5%, which was concluded to be a fairly small and acceptable uncertainty for the assumption of a flat rotation curve.

The uncertainty associated with calculation of the column density is dominated by the conversion values chosen. For ^{12}CO the widely accepted W_{CO} value (Dame et al. 2001) is used, with a 10% uncertainty to account for any variations in the uniformity of the tracer in the region. The abundance ratios and X values for ^{13}CO, $C^{18}O$, and HCO^{+}

are much more uncertain and can range greatly based on various assumptions. This has been taken into account and the uncertainties have been adjusted accordingly. Since the HCO^{+} is the most uncertain, a factor of 3 error for the abundance ratio (Barnes et al. 2011) is applied. The ^{13}CO X-factor has a wide degree of variance dependent on local properties and the amount of star formation in the region (Pineda et al. 2008). A wide range of X-factors have been derived and in comparison to this study the following are applied: a factor 2 uncertainty for the ^{13}CO and a factor 2.5 uncertainty for the $C^{18}O$ (Pineda et al. 2008, Glassgold et al. 1985).

One other source for uncertainty in calculating the column density is the error introduced by integration of the brightness temperature over the velocity range. For the Nanten data the sensitivity appears to be deep enough to get a very low rms per channel. As a result the integration errors were very close to zero. The HI shows the same negligible errors.
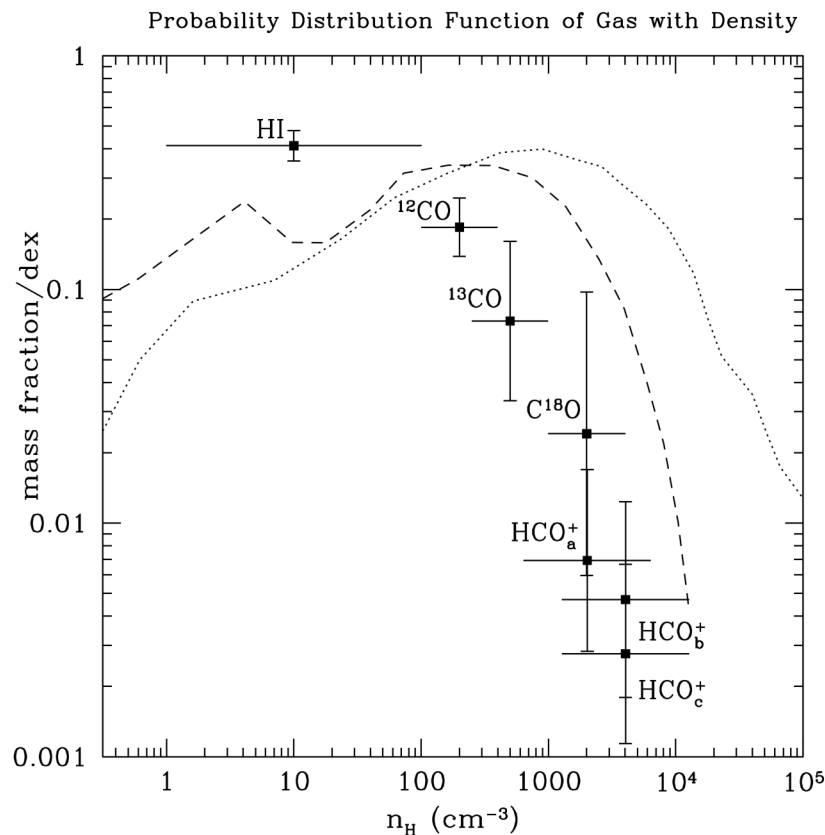

Figure 1: Gas Density PDF for the HI & H₂ in the CHaMP region. Plotted black squares represent the fraction per dex for each tracer at the center of their estimated density range. Horizontal bars indicate the range of densities each covers, and the vertical bars span the uncertainty range we have calculated for each. The dotted line represents a model gas density PDF with no FUV heating feedback from a simulation from Tasker & Tan (2009). The dashed line is a model run by Tasker (2011) that includes the FUV *heating*.

The combined errors are plotted as the vertical axis bars for the observed mass fraction values in Figure 1. The HI and the ^{12}CO have the least amount of error, mostly due to the minimization of uncertainty in their calculations and conversions. The remaining molecular tracer errors exhibit the level of uncertainty that exists. The mass fractions are plotted against a simulated galaxy's mass fractions (Tasker & Tan 2009; Tasker 2011) as a rough comparison. The simulation was modeled to create a galaxy similar to the Milky Way that can be used to study GMC evolution and is plotted against the observed gas density PDF in Figure 1. The dotted line shows a PDF from the simulation of Tasker & Tan (2009) that did not include FUV heating, while the dashed line includes those effects. The model with no FUV heating assumes a flat rotation curve and does not include star formation and feedback, but instead it focuses on gravitational instabilities and cloud collision effects.

With the inclusion of the heating, the model estimates an overabundance of mass over the ^{12}CO and ^{13}CO density range. The higher density observations covered by $C^{18}O$ and HCO^+ do drop off sharply and appear to match the drop of the model near the Paper I sources' mass weighted density average of 4.0×10^3 cm^{-3}.

The gas density PDF also includes points from the comparison analysis between the Mopra and Nanten data. As shown in Table 2, the total mass of the CHaMP sources from Paper I as calculated through a two dimensional Gaussian fit is 0.219 x 10^6 M$_\odot$ and is plotted as the point

$HCO+_c$ in Figure 1. Calculating the summed intensity in an ellipse twice the size of the half power ellipses defined from the Paper I yields a total mass of 0.263 x 10^6 M$_\odot$. Yet this value may be double counting mass if nearby ellipses are overlapping. While the majority of sources are mostly isolated, there are certain regions that have numerous sources overlapping. A future fix to this could be to develop a routine that determines overlapping pixels in three dimensional space, and then assigns the mass in that pixel to the closer source. The expected result would lead to a mass that would approach the two dimensional Gaussian total mass. The HCO^+_a point in Figure 1 shows the total mass calculated from the Nanten cubes, 0.541 x 10^6 M$_\odot$. This used the method of taking overlapping regions from the CHaMP HCO^+ survey and setting them to the equivalent distances of the sources in the corresponding region in order to minimize distance ambiguities. A separate point, HCO^+_b shows only the mass from the Nanten survey that overlaps with the regions in longitude space covered by Paper I. This value of the Nanten mass, 0.336 x 10^6 M$_\odot$, differs from the Paper I full region total by ~7 x 10^5 M$_\odot$. The beam size of Nanten compared to Mopra would lead to some undersampling, but as Paper I discusses, barely 2% of the CHaMP sources could be considered point like. Therefore we conclude that the majority of the extra mass seen is most likely from low level emission in widespread low density clumps.
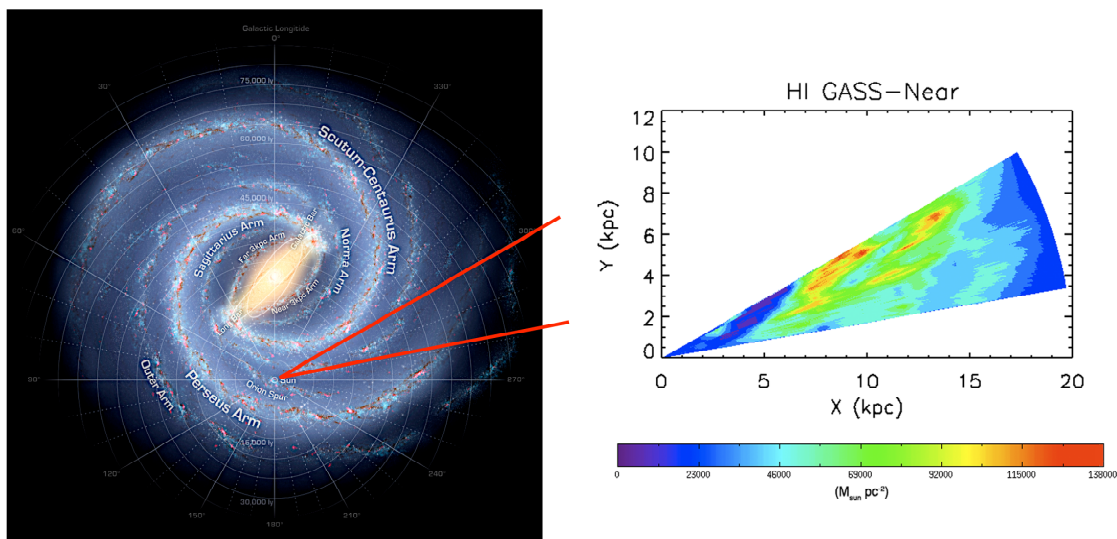

Figure 2: On the left, an artist's conception of the Milky Way as viewed from above. The red lines outline the CHaMP region in longitude, from 280° to 300°. Source: NASA/JPL Caltech/R. Hurt (SSC-Caltech). On the right, a mass surface density map of the region as viewed from above based on the HI GASS survey covering a distance out to 20 kpc and assuming near distances for the distance ambiguity.
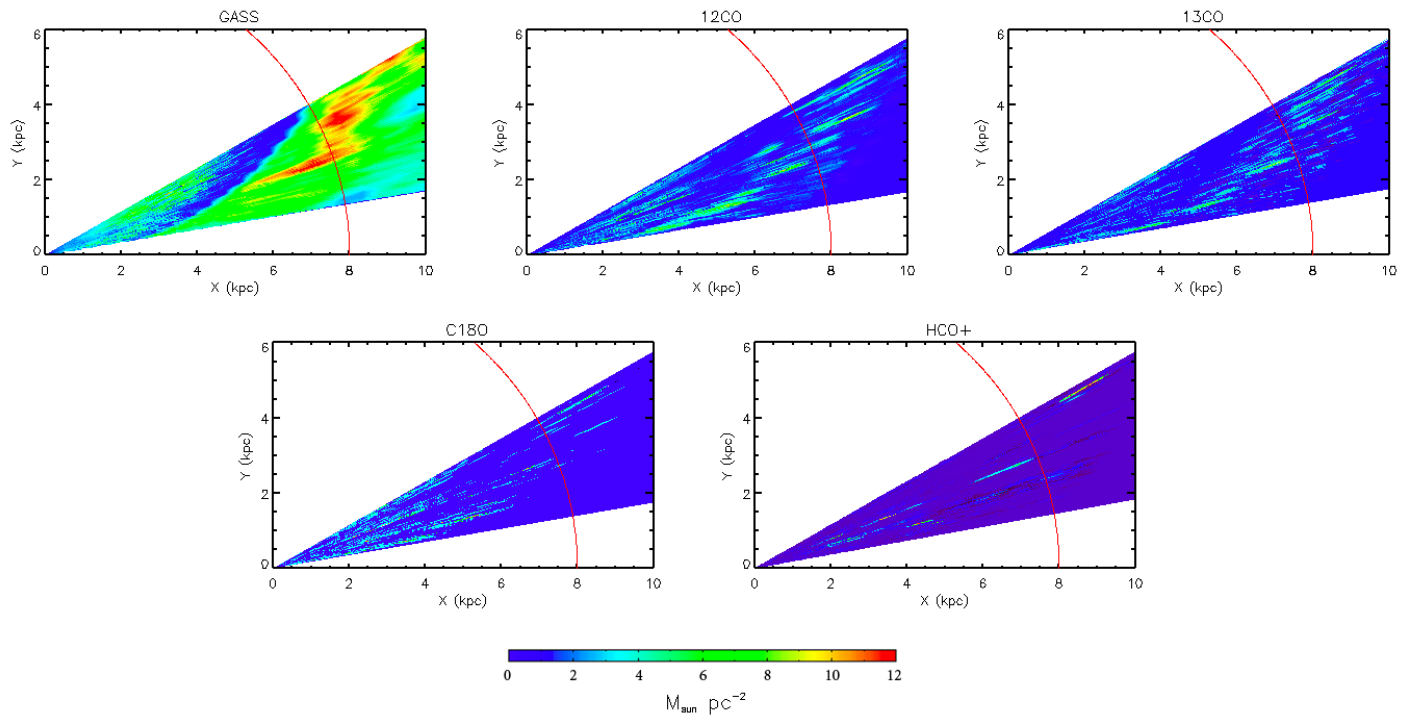
Figure 3: Maps for HI and the H$_2$ molecular tracers of the mass surface density over the CHaMP region (280° to 300°), out to 10 kpc. The red line represents the radius cutoff of 8 kpc imposed in creating the gas density PDF.

The final part of this research focuses on visualizing the results. When calculating the mass totals for each survey, the distance was divided up into 0.5 by 0.5 kpc boxes along each longitude in order to create overhead maps of the mass surface density. Figure 2 shows the latest artistic representation of the Milky Way as viewed from above (*NASA/JPL Caltech/R. Hurt (SSC-Caltech)),* with an outline of the CHaMP region. On the right is the first of the overhead maps, from the HI GASS survey. For simplicity, all the maps assume the near distance ambiguity. The Carina Arm is quite visible in the map as the regions that have the greatest mass surface density trace out a distinct spiral arm pattern. Figure 3 displays the GASS HI and all the Nanten H$_2$ tracers, out to a distance of 10 kpc.

Conclusions

The atomic and molecular hydrogen was studied in a 20° by 6° region of the Milky Way in order to derive a gas density PDF. This region coincides with the area covered by the CHaMP survey and will allow for further insight into the study of star formation and GMCs. The results confirm the expectation that the majority of gas in the local region is mostly atomic hydrogen. The mass estimates required addressing the distance ambiguity brought about by any sources that fell within the solar radius. Basing the distance calculation only on the velocity of the source, two mass calculations were run to get an upper and lower limit.

These were averaged and combined with the mass outside the solar radius for the final mass totals.

In constructing the gas density PDF, uncertainties from the ambiguity as well as uncertainties due to conversion factors of the tracers to H$_2$ and any Y & X factors used in the column density calculations must be taken into account. The HI and ^{12}CO have the least amount of uncertainty compared to the other tracers, which is key since they account for a large percentage of the mass for the region. It should be noted that the mass results for the ^{13}CO are slightly lower than expected and are in fact a lower limit since they are based on the assumption of being optically thin. Also, the HCO$^+$ conversion factor to H$_2$ is uncertain and as a result the mass fraction varies by a factor of three.

The observed gas density PDF was also compared to simulated gas density PDFs of a galaxy with and without FUV heating feedback. There is a general agreement with the FUV heating model, though the model has too much mass in the density ranges covered by ^{12}CO and ^{13}CO. However, this model has a steeper drop off at the C^{18}O and HCO$^+$ densities that roughly corresponds with the observed values.

Comparison of the CHaMP source mass total to the complete total covered by the Mopra and Nanten cubes leads to the conclusion that there is fair amount of low density gas at fainter emissions that is contributing to the gas mass.

Further work will be done to investigate and reduce the uncertainty in the density ranges for each of the molecular tracers in the gas density PDF. Future galaxy simulations could eventually lead to a tighter correlation between observed and modeled PDFs. Additional research can build from this project to solve the distance ambiguities that arise. By using the defined clumps from the CHaMP region we can study the HI data from the SGPS survey to possibly eliminate the distance ambiguity by checking for HI self-absorption features (Goldsmith & Li 2004). These absorption features are the result of a cold HI cloud that is in front of a warmer HI cloud (Anderson & Bania 2009). Several studies have shown that molecular clouds generate these HI self absorption features, and it is generally agreed that evidence of these features at the same velocity and velocity width as the molecular tracers means the cloud is at the near distance (Anderson & Bania 2009).

References

Anderson, L. D., Bania, T. M., 2009, ApJ, 690, 706

Barnes, P. J., Yonekura, Y., Ryder, S.D., Hopkins, A. M., Miyamoto, Y., Furukawa, N., Fukui, Y., 2010, MNRAS, 402, 73

Barnes, P. J., Yonekura, Y., Fukui, Y., Miller, A. T., Mühlegger, M., Agars, L. C., Miyamoto, Y., Furukawa, N., Papadopoulos, G., Jones, S.L., Hernandez, A. K., O'Dougherty, S. N. Tan, J. C., 2011, ApJ, submitted

Dame, T. M., Hartmann, D., Thaddeus, P., 2001, ApJ, 547,792

Fukui, Y., Kawamura, A., Minamidani, T., Mizuno, Y., Kanai, Y., Mizuno, N., Onishi, T., Yonekura, Y., Mizuno, A., Ogawa, H., Rubio, M., 2008, ApJS, 178, 56

Goldsmith, P.F., Li, D., 2004, ApJ, 622, 938

McClure-Griffiths N. M., Dickey, J.M. Gaensler, B. M., Green, A. J., Haverkorn, M., Strasser, S. 2005, ApJS, 158, 178

McClure-Griffiths N. M., Pisano, D. J., Calabretta, M. R., Ford, H. A., Lockman, F. J., Staveley-Smith, L., Kalberla, P., Bailin, J., Dedes, L., Janowiecki, S., Gibson, B. K., Murphy, T., Nakanishi, H., Newton-McGee, K. 2009, ApJS, 181, 398

Reid, M. J., Menten, K. M., Zheng, X. W., Brunthaler, A., Moscadelli, L., Xu, Y., Zhang, B., Sato, M., Honma, M., Hirota, T., Hachisuka, K., Choi, Y. K., Moellenbrock, G. A., Bartkiewicz, A., 2009, ApJ, 700, 137

Rohlfs K. & Wilson T.L. 2006, Tools of Radio Astronomy, 4th ed. (Springer: Berlin)

Pineda, J. E., Caselli, P., Goodman, A. A., 2008, ApJ, 679, 481

Spitzer, L. Jr., 1978, Physical Processes In The Interstellar Medium, (John Wiley & Sons: New York)

Tasker, E., Tan, J., 2009, ApJ, 700, 358

Tasker, E. 2011, ApJ, 730, 11

Yonekura, Y. Asayama, S., Kimura, K., Ogawa, H., Kanai, Y., Yamaguchi, N., Barnes, P.J., Fukui, Y., 2005, ApJ, 634, 476